Improving the seismic behaviour of RC frames with mortarless blocks

Authors:

[1]Assist.Prof. **Hakan Koman**
hakankoman@aydin.edu.tr
Corresponding author

[2]Assoc.Prof. **Halil Nohutcu**
halil.nohutcu@cbu.edu.tr

[3]Prof. **Gökhan Kılıç**
gokhan.kilic@ieu.edu.tr

[4]Prof. **Arkadiusz Kwiecien**
arkadiusz.kwiecien@pk.edu.pl

[5]Assoc.Prof. **Emre Ercan**
emre.ercan@ege.edu.tr

[1] Istanbul Aydin University, Istanbul, Turkey
Faculty of Engineering
[2] Manisa Celal Bayar University, Manisa, Turkey
Faculty of Engineering
[3] İzmir Economical University, İzmir, Turkey
Faculty of Engineering
[4] Krakow University of Technology, Poljska
Faculty of Engineering
[5] Ege University, İzmir, Turkey
Faculty of Engineering

Hakan Koman, Halil Nohutcu, Gökhan Kılıç, Arkadiusz Kwiecien, Emre Ercan

Improving the seismic behaviour of RC frames with mortarless blocks

This paper investigated the effects of mortarless blocks on a reinforced concrete (RC) frame based on computational and experimental analyses by comparing its behaviour with those of traditional frames with and without walls. The effects of the joint between the wall and frame were investigated using flexible and stiff joints. The use of a flexible joint prevented segregation between the wall and frame. The frame with traditional infill had increased lateral rigidity (1.44 times of the bare frame). A dry stack wall with mortar between the wall and frame increased the lateral rigidity by 1.25 times. The frame with the polymer exhibited a behaviour similar to that of the bare frame, especially with respect to the initial stiffness. In the computational analysis, in which the lateral drift of the RC frames was as high as 0.08, it was concluded that the mortarless masonry allowed a 17 % increase in load capacity compared with that of the bare frame. The dry stack masonry increased the lateral stiffness of the bare frame by only 10 %, whereas the traditional infill wall increased the stiffness of the bare frame by 1.42 times in computational analysis. When a polymer was used between the dry stack wall and frame, the stiffness was similar to that of the bare frame. Thus, dry-stack masonry walls with different gap fillers can be used to increase the period of structures as an alternative approach to earthquake-resistant structural design. The use of a polymer decreased the wall damage by reducing the stresses and allowed the highest lateral drift. Compared with the RC frame without walls, the dry-stacked masonry-infilled frame with the polymer binder was slightly more ductile.

Hakan Koman, Halil Nohutcu, Gökhan Kılıç, Arkadiusz Kwiecien, Emre Ercan

Poboljšanje ponašanja AB okvira s blokovima bez morta pri potresu

U ovom su radu istraženi učinci blokova bez morta na armiranobetonski (AB) okvir na temelju proračunskih i eksperimentalnih analiza, uspoređujući njegovo ponašanje s ponašanjem tradicionalnih okvira s ispunskim zidovima i bez njih. Utjecaj sljubnica između zida i okvira istražen je razmatranjem fleksibilnih i krutih sljubnica. Primjena fleksibilne sljubnice spriječila je odvajanje zida i okvira. Okvir s tradicionalnom ispunom imao je povećanu bočnu krutost (1,44 puta u odnosu na okvir bez ispune). Suhozid s mortom između zida i okvira povećao je bočnu krutost 1,25 puta. Okvir s polimerom pokazao je slično ponašanje kao okvir bez ispune, posebno u pogledu početne krutosti. U proračunskoj analizi, u kojoj je bočni pomak AB okvira iznosio čak 0,08, zaključeno je da je zidanje bez morta omogućilo 17-postotno povećanje nosivosti u usporedbi s nosivosti okvira bez ispune. Suhozidom se bočna krutost okvira povećala za samo 10 %, dok je tradicionalni ispunski zid povećao krutost okvira 1,42 puta u proračunskoj analizi. Kada je između suhozida i okvira primijenjen polimer, krutost je bila slična krutosti okvira bez ispune. Zato se suhozidi s različitim ispunama mogu primjenjivati za povećanje osnovnog perioda konstrukcije kao alternativni pristup projektiranju konstrukcije otporne na potres. Primjenom polimera smanjilo se oštećenje zida smanjenjem naprezanja te je omogućen najveći bočni pomak. U usporedbi s AB okvirom bez ispune okvir s ispunom od suhozida i polimernim vezivom bio je nešto duktilniji.

1. Introduction

Many destructive earthquakes have occurred worldwide, including those reported in Kocaeli (1999), Northridge (1994), Kahramanmaras (2023), Landers (1992), and Kobe (1995). Many people were killed and economic damage occurred because of the destruction of buildings. In particular, non-ductile moment-frame structures are risky. Increasing the energy dissipation in buildings is required to overcome the destructive effects of strong ground motions. Seismic dampers have been used to achieve this goal, and their properties have been developed. Frictional, metallic yielding, viscous, and viscoelastic dampers are passive energy dissipation devices that have been used in previous studies. This type of energy dissipation device is an economical and alternative solution for the seismic retrofitting of buildings compared with traditional seismic retrofitting methods, such as the use of reinforced concrete (RC) walls to increase the lateral stiffnesses of structures. In a seismic retrofit analysis of a building in Istanbul, it was shown that using frictional damper devices is a more feasible alternative than traditional retrofit methods because of the ease of device placement without disturbing residents or forcing them to move during the retrofit process [1]. In another study, an analysis was performed using frictional dampers. When steel braces with frictional dampers were added to existing frames, the horizontal strength and rigidity increased, moment loads on the columns decreased, and column axial forces increased. RC walls behaved rigidly under shear loading and were disadvantageous when frictional dampers were used because they could not provide the necessary displacement. The friction load that activates frictional dampers can be selected such that the structure can maintain elastic behaviour under the expected effects, such as wind and small ground motion [2]. In another study, three types of metallic dampers were proposed. The analysis was conducted by adding dampers to existing steel and reinforced concrete structures. Among the introduced dampers, the highest energy consumption was for the hybrid damper using metallic yielding and friction (MYFD). According to a study conducted on an actual RC building, an MYFD-type damper reduced the structural response by approximately 35 % [3]. Dampers can improve the seismic performance of structures; however, their construction cost prevents them from becoming popular.

In seismic areas, infill walls in frames are typically used as shelters, and the division of space and their effects on the structure's earthquake behaviour have been neglected in past designs. However, in reality, walls can change the stiffness, period, and ductility of a structure during a strong earthquake owing to the interaction between the wall and frame. In addition, infill walls can fail in the out-of-plane direction at any time during an earthquake, which can unexpectedly change the behaviour of the structure. Infill walls can cause differences in lateral stiffness between stories and create soft-story irregularities. Many researchers have investigated these problems and used fictitious compressive struts to model the wall behaviour. This approach has also been adopted by seismic codes such as Eurocode 8 and Federal Emergency Management Agency 356 [4].

Conversely, transforming walls that have already been constructed for non-structural reasons into energy dissipators is a reasonable idea. An experimental study concluded that dry-stack panels can improve considerably seismic energy dissipation when the frame is in the elastic stage without increasing the stiffness of the frame [5]. Therefore, in another study, a dry stack panel was modelled as an energy dissipation device, and the Jacobsen approach was used to calculate a new damping ratio for the dynamic analysis of the frame [6]. In Jacobsen's approach, the damping ratio for the nonlinear stage of the structural behaviour was calculated by proportioning the energy dissipated by the device to the elastic strain energy of the frame. It was also stated that the joint (between the frame and dry-stack panel wall) properties (irrespective of whether there was a gap between the panel and frame) changed the energy-dissipation characteristics of the frame. In another study, different types of gap fillers were used, and it was observed that a rigid joint between the dry stack panel wall and the frame caused more energy dissipation in the frame under lateral loads compared with their counterparts, including foam as a joint. This was caused by the vertical movement of the infill during the lateral loading of the frame. The foam allowed the infill to move more vertically; however, in its rigid counterpart, more friction acted between the mortarless blocks which allowed the frame to carry more lateral load and dissipate more energy [7]. In another study, the damping ratios of the frames with dry-stack walls were calculated. A damping ratio of 0.03 was found for the frame without walls. A damping ratio of 0.17 was found for the frame with a dry stack masonry infill. Theoretically, if the friction coefficient between the bricks can be increased, this damping will increase further. According to their results, a frame with mortarless walls consumes more energy than a frame with traditional infill walls or a bare frame [8].

In another study, simplified numerical modelling was performed using the *Seismostruct* software's inelastic wall modelling approach, after a detailed finite element method (FEM) analysis with DIANA, and it was concluded that semi-interlocking dry-stacked masonry is beneficial for improving the energy dissipation of the structure without reducing considerably the displacement ductility [9].

In a previous experimental study, it was shown that after the failure of columns owing to axial loads, semi-interlocking masonry helps frames carry axial loads and continues to dissipate energy owing to friction between blocks in the inelastic stage of frames. The frames with semi-interlocking masonry walls had a lateral load-carrying capacity approximately 1.4 times larger than that of the bare frame without any infill wall. The authors observed fictitious weak diagonal compressive strut behaviour in a semi-interlocking brick masonry infill under lateral loading of the frame [10].

In Türkiye, a study was conducted with local semi-interlocking hollow bricks; however, in that study, the frame's lateral load

capacity did not increase when compared with that of a bare frame without any infill wall [11]. This can be related to the fact that the use of hollow bricks caused weak resistance when the dry-stacked wall acted as a fictitious compressive strut, and this did not help the frame increase the lateral load capacity.

In another study, mortarless masonry systems proposed by two teams from two countries were compared. For this purpose, the cyclic test results of the infilled walls were first calibrated in the numerical analysis to model the mortarless walls as equivalent compressive struts. Subsequently, non-linear static and non-linear time history analyses were conducted on a six-storey frame. The results showed that the mortarless masonry proposed by the University of Pavia team increased the capacity by 1.6 times when compared with the bare frame without infill walls [12].

In another study, the response reduction factors for RC structures with semi-interlocked and unreinforced masonry infills were compared with those for bare frames. A push-over analysis was conducted for four-storey structures. They concluded that in all cases of semi-interlocking masonry infill placement in the structure, the response reduction factor was higher than that of the bare and unreinforced masonry frames [13].

Conversely, the flexible joint method showed that using highly deformable adhesives for joints reduces stress concentrations and improves the load-carrying capacity of the joints [14]. In previous experiments, bricks repaired with flexible adhesives withstood more load than their non-deformed counterparts in flexure tests, although the tensile strength of the adhesive was lower than that of the bricks [14]. Other researchers subsequently concluded that the use of flexible joints increased the energy dissipation capacity of structures [14-17]. In these studies, it was stated that highly deformable adhesives for flexible joints could be modelled as hyperelastic materials, and the mechanical properties of the highly deformable adhesive were given [14-17].

In another study, polymer injection was used between traditional hollow brick-RC frame interaction zones. In the in-plane shear test of frames, polymer injection was observed to make the frame more ductile; however, at a lateral drift of 1.6 %, the interaction failed, deven though the polymer injection prevented out-of-plane collapse of the wall [18]. In another study, shaking table tests revealed that polymer injection protected the traditional infill and delayed the failure of the interaction zone until a 2.5 % lateral drift [19]. These results were confirmed by those of another experimental study, in which the structure was able to withstand strong harmonic vibrations at the shake table for a long duration (10 min) (1.35 g, 30 mm, 1.3 % lateral drift) [20].

This study aims to investigate dry-stacked masonry as an energy-dissipating wall system inside an RC frame. The use of dry-stack masonry inside RC frames changes their capacity and rigidity. In the earthquake-resistant design of structures or during a seismic retrofitting process, decreasing the rigidity of frames compared with traditional infill walls can be beneficial. As indicated in a previous study [7], the interaction between dry-stacked masonry and the frame causes a clamping zone in the wall, and friction

between bricks occurs inside that zone. If the interaction is stopped by a gap between the frame and masonry, the clamping zone is cancelled; thus, the energy dissipation decreases. Therefore, the aforementioned highly deformable adhesives can be advantageous for providing a ductile contact zone between the wall and frame without allowing any separation of materials. Highly deformable adhesives can decrease the lateral rigidity of the frame compared with rigid gap filler alternatives. Thus, the current study also aimed to investigate the effects of a flexible joint between the frame and mortarless infill on the behaviour of the structure through experimental quasi-static loading of RC frames and FEM analysis using Abaqus [21]. Abaqus was chosen for the computational modelling programme because it provides a powerful approximation of the experimental results [22].

2. Materials and methods

Four RC frames were constructed for the experiment. The frame elements had dimensions of 12 × 12cm dimensions. The frame samples had a height of 0.75 m and a width of 1 m between the inner sides of the columns. A foundation with a cross-section of 30 × 30 cm and a length of 1.5 m was constructed to provide fixed support for the columns. Longitudinal rebars (4Ø8) were used inside the columns and beams, whereas Ø6 rebars were used as confinement rebars. To investigate their behaviour, quasi-static experiments were performed. In the inner parts of three RC frames, different types of infill walls were constructed. One infill wall was a traditional infill wall for comparison and it was constructed with mortar and ordinary hollow bricks (dimensions of 190 × 85 × 100 mm). The other two infill walls were both dry stack masonry constructed using 190 × 90 × 50 mm solid clay bricks which are used in practice for masonry construction. Different joint materials were used between frames and dry stack walls. Flexible and rigid joints were created by using Polymer PM and mortar, respectively.
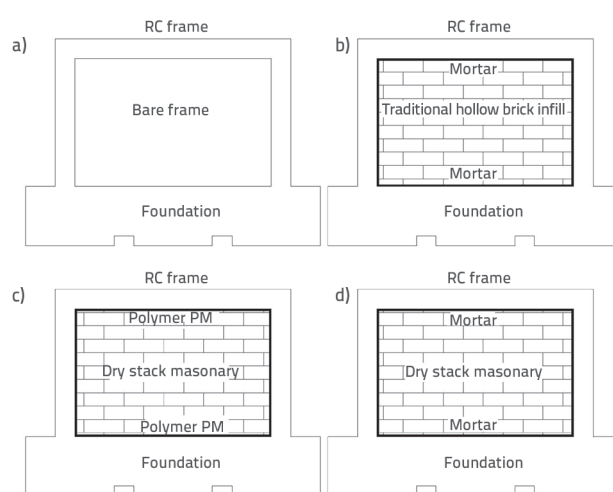
Figure 1. Schematic views of: a) bare frame; b) frame with traditional infill; c) frame with dry-stack masonry and polymer binder; d) frame with dry-stack masonry and mortar

2.1. Material tests

The compressive strength of the concrete used in the frame was determined via compression tests. The average 28-d compressive strength of the cubic specimens was 30.25 MPa. Therefore, the concrete can be classified as C25/30 according to the TS-EN 206 standard.

The tensile test results showed that these were intended for the steel rebars used inside the frames. The yield and tensile strengths of the B420C used as 8 mm bars in the RC frame were assumed to be 491 MPa and 553 MPa, respectively. Regarding B420C used as a 12 mm bar, the yield and tensile strengths were assumed to be 490 MPa and 610 MPa, respectively. SAE 5.5 mm steel (SAE 1008 steel) was used as confinement in the RC frame with the yield and tensile strengths assumed to be 277 MPa and 387 MPa, respectively. The elongation of the SAE steel was 42 %.

The mortar used in the experiments was a 1:2:9 (cement:lime:sand) mortar consisting of class CEM 1 32.5 Portland cement and hydrated lime. The amount of water required to provide a 10 mm flow rate was obtained. Compression and flexural tests were conducted according to the TS EN 196-1 standard. For the tests, 40 mm × 40 mm × 160 mm beam specimens were prepared. To obtain the modulus of elasticity of the mortar, a 100/200 mm cylindrical specimen was prepared, and tests were performed according to EN 13286-43. The average densities of the six mortar specimens were 1954.14 kg/m³. In the flexural tests, the loading speed was 50 N/s and the distance between the supports was 100 mm. The average flexural strength of the mortar was 0.257 MPa. The compressive tests performed on half of the specimens after the flexural tests revealed an average strength of 5 MPa. The modulus of elasticity was experimentally obtained, but the results were invalid owing to a camera error that occurred during the strain measurement; therefore, the modulus of elasticity was obtained from a previous experimental study [23] performed for the same type of mortar. In a previous study, it was concluded that the values of the mortar hardened between bricks should be considered representative of the actual situation in masonry, and the average modulus of elasticity was found to be 700 MPa [23].

To simulate the behaviour of the frame in the computational model, it is important to understand the behaviour of the mortar-brick transition zone. Thus, three specimens were prepared for the shear and tensile failure modes of the bonds between mortar and brick. However, the results of specimen 3 in the shear test contained errors owing to the vibration that occurred in the camera, which was not used. The mortar–concrete transition zone was assumed to exhibit the same behaviour in the numerical analysis of the dry-stack masonry. Figure 2 shows the shear and tensile failure mode tests. Steel plates on the specimens were used to create smooth surfaces during loading. The loading speed during the shear test was set to 10 N/s. After loading, a stress–displacement graph was obtained for each specimen. Figure 3 shows the results of the tensile bond tests.
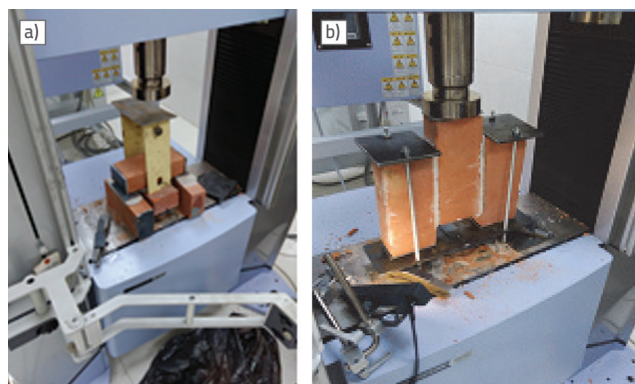
Figure 2. a) Tensile tests; b) Shear bond tests

Figure 4 shows the results of the shear-bond tests in which the fracture energy in the corresponding mode was obtained by calculating the area under the graphs. In shear-bond tests, the areas under the graphs for specimens 1 and 2 were found to be 0.21 MPa and 0.15 MPa, respectively. In tensile bond tests, the areas under the graphs of specimens 1, 2, and 3 were found to be 0.14 N/mm, 0.06 N/mm, and 0.12 N/mm, respectively. The average shear fracture energy was 0.18 N/mm and the average tensile fracture energy was found to be 0.10 N/mm.

Two types of clay bricks were used in the experiments. Clay bricks produced for masonry construction were used in mortarless walls. Hollow clay bricks are commonly used for traditional infill walls. According to TS EN 772-1, the compressive strength of the masonry bricks was determined to be 16 MPa. The average tensile strength of the masonry bricks was determined to be 8.94 MPa in the flexural experiments (Figure 5).
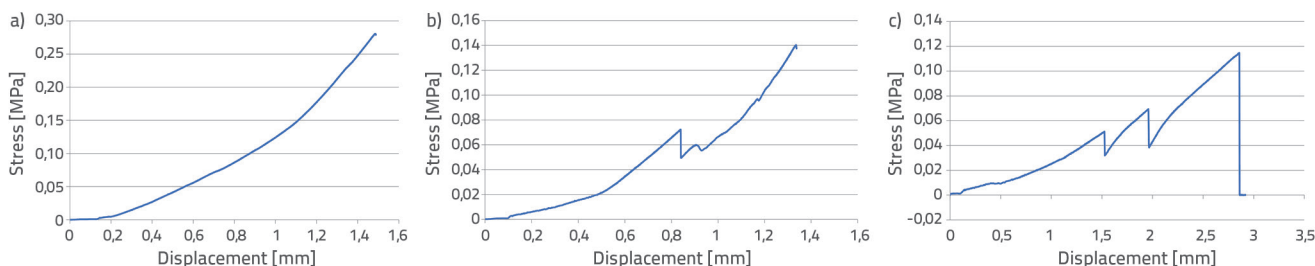
Figure 3. Tensile bond tests of samples: a) Sample 1; b) Sample 2; c) Sample 3

a)

b)
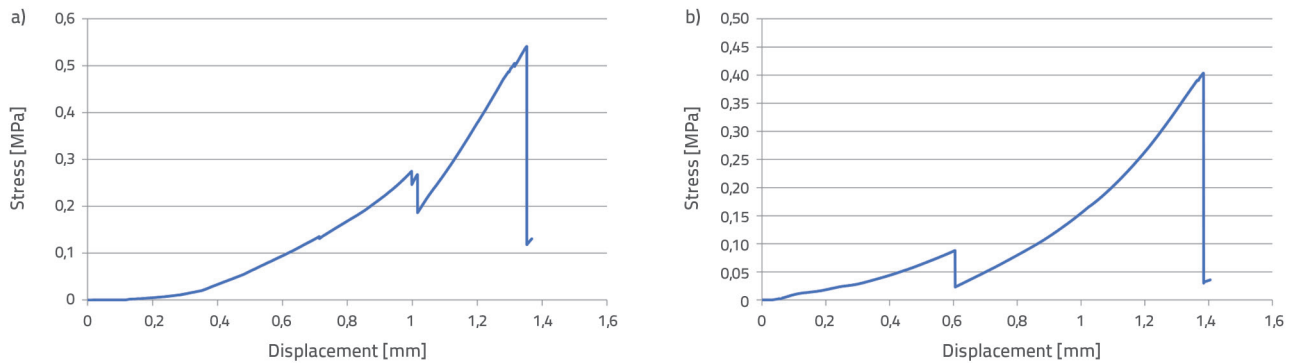
Figure 4. Shear bond test of samples: a) Sample 1; b) Sample 2

Figure 5. a) Bending test of the hollow brick specimen;). Bending test of the clay brick specimen;). Compression test of the hollow clay brick

The elasticity modulus of the masonry-type brick was set to 6000 MPa, as indicated in a previous study [24]. The compressive strength and elasticity modulus of the hollow bricks were determined using a compressive test (Figure 5). The loading speed during the test was 0.15 MPa/s and a steel plate with epoxy resin was applied at the top and bottom surfaces of the brick to obtain uniform loading. The strain in the middle zone was measured using a camera; the average compressive strength of the hollow brick was 3.56 MPa and the average modulus of elasticity of all hollow brick specimens was 1111 MPa. The tensile strengths of the hollow bricks were calculated using bending tests. The average tensile strength of all the hollow brick specimens was 0.9 MPa.

2.2. Frame cyclic tests

2.2.1. Frame properties

A frame with a 40 × 40 cm column beam was designed in accordance with the RC member design rules of the 2018 Turkish seismic code (TSC 2018) [25]. It had a height of 3 m and a width of 4 m and was designed based on lateral and vertical column loads of 250 kN and 600 kN, respectively. After structural analysis, the following internal forces were obtained for the RC design, N_d = 700 kN (axial), V_d = 126 kN (shear), M_d = 206 kNm (moment) for the column and V_d = 92 kN, M_d = 172 kNm for the beam. The longitudinal rebars of the beam and

column were designed according to the internal forces, and the rebar area was determined by determining the maximum and minimum ratios from TSC 2018 [25]. The capacity design method was used for the confinement rebar analysis, as indicated in TSC 2018 [25]. The capacity design method was based on the use of the plastic hinge moment of the elements and the elimination of the contribution of concrete to the shear resistance during the design of the shear reinforcement. The shear force limit of the code to prevent brittle compressive behaviour was also controlled. Rules for column confinement rebar were controlled and Ø12/10 cm (12 mm) rebars were selected for 40 × 40 cm columns. In column cross-sections, a longitudinal rebar percentage of 0.01141 was determined and the value of 12Ø14 was selected in practice. Owing to the lifting problems of heavy weight frame, the frame was scaled by 1/4 but instead of 10 × 10 cm cross-sections, a frame with 12 × 12 cm cross-sections (for constructive and factory-related reasons) was obtained. This scaling process was performed using practical true modelling laws discussed in previous studies [26, 27]. The practical true model approach outcomes are listed in Table 1. In Table 1, F indicates force, L indicates length, and S_l indicates the scaling ratio (in this study: 4). The RC design was re-checked for the dimension of 12 × 12 cm, and no change was found for the rebars in the design. For example, the required longitudinal rebar area for a 48 × 48 cm column was 2628 mm²; if the rebar areas were divided by a factor of 16, then it was observed that 4Ø8 was suitable for the scaled models of both the 10 ×10 cm and 12 × 12 cm columns (Ø8 is the minimum available rebar in the market). According to the scaling laws, shear reinforcement must also be scaled, but to provide extra-large lateral displacement loading to the frame, extra confinement bars were added to the beam–column joint region of the 12 × 12 cm frame, by following the TSC 2018 approach. According to TSC 2018 [25], the length of this region in beams must be at least two times the beam's height, and the space between confinement rebars in that region in beams must be 0.25 of the beam's height; therefore, a space of 30 mm between successive confinement rebars was selected when the length was 240 mm. Hollow bricks (190 × 190 × 135 mm) are standard bricks. Therefore, it was assumed there was no need to scale
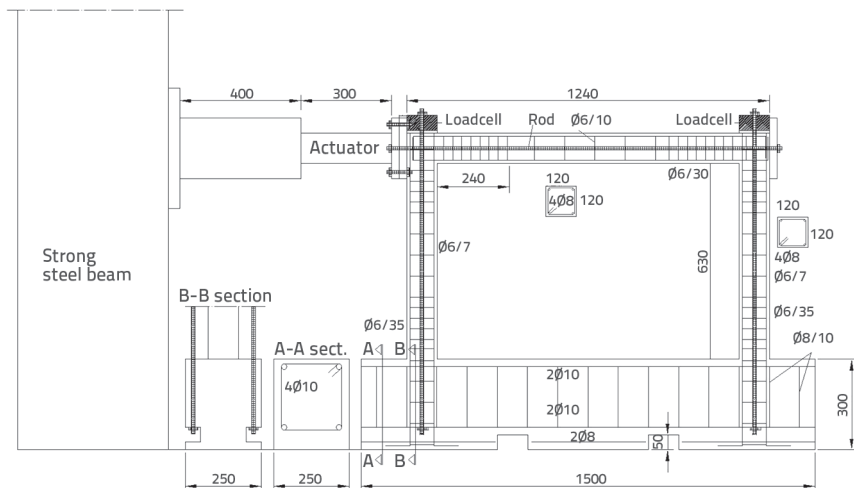
Figure 6. 1/4 Scaled frame and loading conditions in experiments

190 × 85 × 100 mm hollow brick specimens used in traditional wall experiments. In mortarless walls, bricks with heights of 50 mm and widths of 90 mm were used. In this study, the analysed frame does not have strong column-weak beam behaviour; accordingly, this can limit the energy dissipation due to friction in dry stack masonry. The frame details and dimensions in mm are shown in Figure 6. The concrete cover was 15 mm. The design was used in a previous numerical study [28].

Table 1. Practical true model [26]

Quantity	Dimension	Practical true model
Concrete stress	FL^{-2}	1
Concrete strain	-	1
Concrete's modulus of elasticity	FL^{-2}	1
Concrete's Poisson's ratio	-	1
Unite volume weight	FL^{-3}	$1/S_l$
Rebar stress	FL^{-2}	1
Rebar strain	-	1
Rebar's modulus of elasticity	FL^{-2}	1
Adherence stress between rebar and concrete	FL^{-2}	1
Length	L	S_l
Displacement	L	S_l
Angular displacement	-	1
Rebar area	L^2	S_l^2
Point load	F	S_l^2
Line load	FL^{-1}	S_l
Pressure	FL^{-2}	1
Moment	FL	S_l^3

2.2.2. Cyclic tests

The loading equipment is shown in Figures 6 and 7. An actuator was used for the cyclic quasi-static test of the RC frames. The horizontal actuator was a servo-controlled actuator with a capacity of 500 kN and a stroke of 250 mm. It was manufactured by a University engineering firm [29]. Potentiometers were placed at the corners of the frame and at the middle height of the columns to measure the lateral displacements. The potentiometers were manufactured by OPKON [30]. Load cells were used to measure the vertical loading of the columns. Lateral loads were applied using a hydraulic actuator with a capacity of 30 cm fixed to the main steel frame. A hinge is placed at the end of the actuator. The frame specimen was placed in a loading system, which is a steel frame with a width of 6.25 m and a height of 3.25 m. Load cells were placed to measure the vertical and lateral loads. The maximum vertical load applied to the columns was 75 kN (uniform pressure approximately equal to 5 MPa), which is the maximum load that can be applied using a rebar fixed on a foundation with tightened nuts. According to the practical true model approach for scaling, additional weights should be placed on the frame; however, the weight of the frame was a small proportion of the total vertical load, so additional weights were unnecessary. This approach was used in a previous study, in which a scaled RC column was also tested. Because the modulus of elasticity and the acceleration ratios were equal to one, the specific gravity should be considered as $1/S_l$. However, in a previous study, it was recommended that acceleration should not be considered in experiments where dynamic effects are insignificant, such as quasi-static effects [31].

Figure 7. Cyclic test of the bare frame

Linear potentiometers were used to detect lateral displacements in the test. Four linear potentiometers were placed at the top corners in the middle of the frames and another at the foundation. The frame was fixed to the stage

using heavy rods as shown in Figure 7. Lateral loading was performed by increasing the force in 5 kN increments as shown in Figure 8. For loads up to 45 kN, three cycles were applied; subsequently, two cycles were used owing to the gain time. After the last increment, displacements of 60 and 65 mm were also loaded. The foundation of the frame specimen was designed to provide fixed support for the columns and lift them onto the stage.
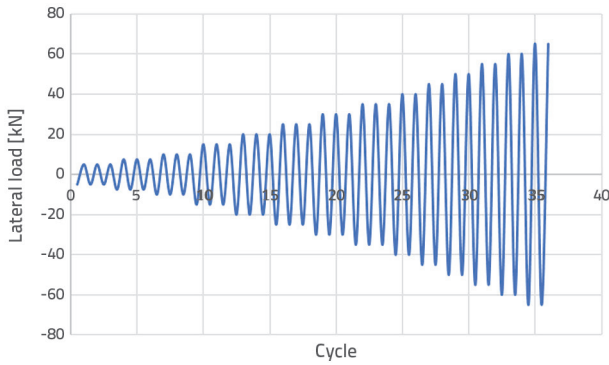
Figure 8. Cyclic test loading

2.3. Computational modelling

2.3.1. Concrete modelling

A concrete damaged plasticity (CDP) computational model was used to model the concrete. The CDP model is a modification of the Drucker–Prager (DP) model. When K = 1, the model is a DP model, as shown in Figure 9 [32]. In contrast to the von Mises theory, the DP theory considers changes in volume owing to hydrostatic pressure to obtain the yield criteria.
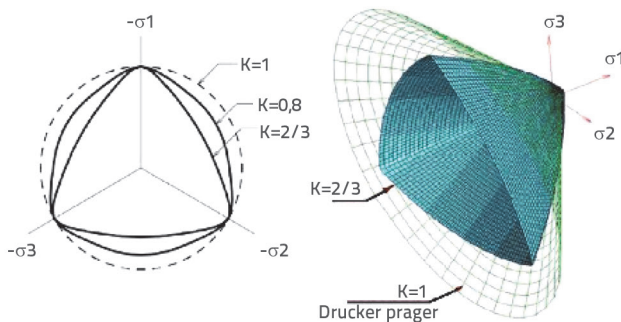
Figure 9. Concrete damaged plasticity model [32]

The stress–strain relationships of concrete in the computational model are shown in Figure 10. In this study, the values on the curve were determined according to Equation 1 [33], and the parameters d_c and d_t, which indicate the effects that deform the elasticity of concrete under compression and tension, were assumed to be zero.

$$f/f_0 = 2.1 \times (\varepsilon/\varepsilon_0) - 1.33 \times (\varepsilon/\varepsilon_0)^2 + 0.2 \times (\varepsilon/\varepsilon_0)^2 \qquad (1)$$

The strain corresponding to maximum stress was assumed to be 0.002 for C25 class concrete, and the Young's modulus was set to 31000 MPa. The dilation angle for the concrete, which indicates the expansion angle calculated in the p–q plane, was set to 38°. This value provides realistic results compared with previous experiments [34]. The eccentricity, which indicates the ratio of the concrete's tensile to pressure strengths, was considered to be 0.1. The value of f_{bo}/f_{co} was set to 1.16, where f_{bo} is the strength of concrete under two-dimensional loading conditions, and f_{co} is the strength under one-dimensional loading conditions.
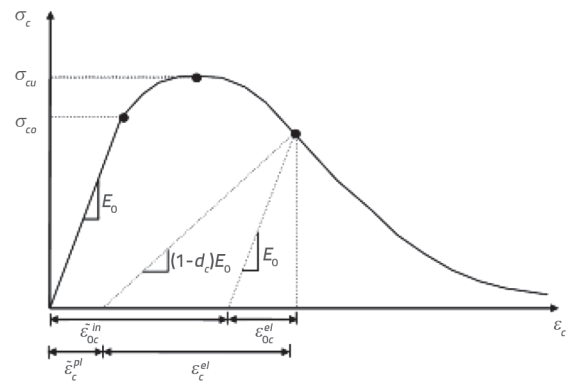
Figure 10. Stress–strain relationship of concrete [34]

2.3.2. Steel modelling

The tensile test results provided by the manufacturers were used to model the behaviour of the steel, as explained in the experimental study in Section 2.1. In the modelling, strain-hardening effects were considered, as expressed in the non-linear modelling section of the Turkish Building Earthquake Code 2018. The stress–strain curves of the steel materials are shown in Figures 11 and 12.
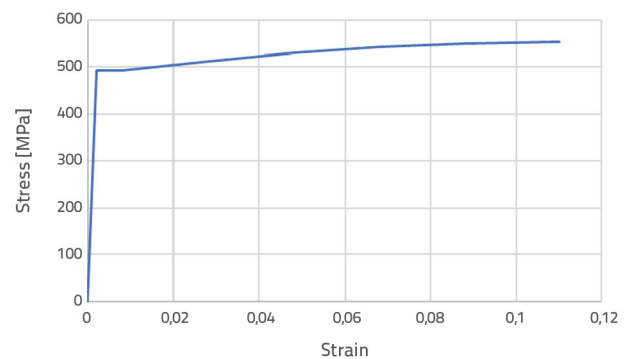
Figure 11 . Stress–strain relationship of S420c steel [25]
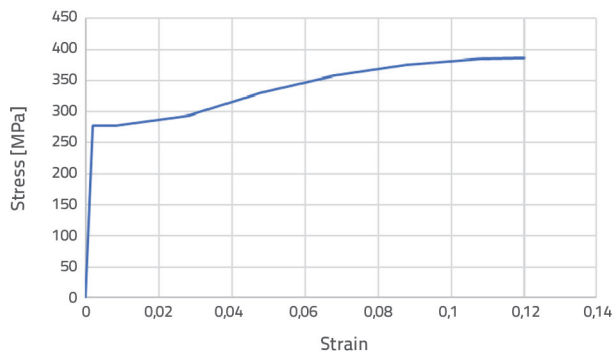
Figure 12. Stress–strain relationship of SAE steel [25]

2.3.3. Modelling of clay bricks

Local bricks were used to model the mortarless masonry (Figure 13). To model the brick behaviour, the CDP model in Abaqus was used by setting the K parameter to one to reflect the DP model.
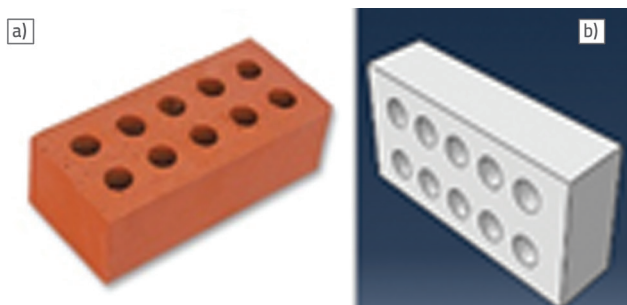
Figure 13. a) Clay bricks used for dry-stack masonry; b) Computational modelling

The stress–strain values were calculated using the parabolic relationship described in a previous study [24]. In this relation, the yield strain in the compressive behaviour was considered as the strain corresponding to 1/3 of the ultimate stress. The stress–strain curves are shown in Figure 14. The mechanical properties of the bricks were determined as described in Section 2.1. A traditional infill wall was constructed using hollow clay bricks, and micro and macro modelling was used.
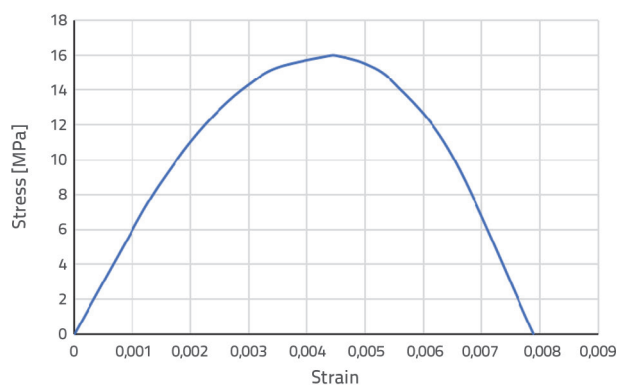
Figure 14. Stress–strain relationships of clay bricks [24]

2.3.4. Modelling of mortar

The CDP model was used to model the mortar behaviour. The dilatation angle was 36.4°. The compressive strength of the mortar, Young's modulus, Poisson's ratio, and tensile strength were found to be 5 MPa, 700 MPa, 0.157, and 0.257 MPa, respectively.

2.3.5. Modelling of polymer binder

Previous studies describing the modelling of the behaviour of flexible materials and discussing the material's mechanical properties [14-16, 35] provided the parameters to be used in the Mooney–Rivlin theory. The Mooney–Rivlin theory is expressed by Eqs. (2–6), as reported in previous studies [14, 35].

$$W^{M-R} = C_{10} \times (\Delta^2 + 2/\Delta - 3) + C_{01} \times (1/\Delta^2 + 2\Delta - 3) \tag{2}$$

$$\begin{aligned} S_1 = F/A_0 = (dW^{M-R}/d\Delta) &= 2 \times (C_{10} \times (\Delta - 1/\Delta^2) + (C_{01} \times (1 - 1/\Delta^2) \\ &= 2 \times (1 - 1/\Delta^2) \times (\Delta\, C_{10} + C_{01}) \end{aligned} \tag{3}$$

$$E_0 = 3G_0 = 6(C_{10} + C_{01}) \tag{4}$$

$$G_0 = 2\,(C_{10} + C_{01}) \tag{5}$$

$$\Delta = L/L_0 = \varepsilon + 1 \tag{6}$$

where L is the final length, L_0 is the initial length, W^{M-R} is the strain energy function of the rubber-like material, S_1 represents stress, E_0 indicates the Young's modulus, G_0 is the shear modulus, and ε describes the strain. C_{10} and C_{01} are the coefficients of the Mooney–Rivlin theory. The calculated values of C_{01} and C_{10} were -0.05 and 0.47, respectively, based on the results of a previous study [36].

2.3.6. Modelling the interaction between binder and materials in the micro modelling approach

Surface-based cohesive behaviour was employed to simulate the interaction between the mortar and bricks, as well as between the polymer and bricks. This approach utilises a simplified method for modelling connections, assuming an extremely thin interface, and adopts a traction-separation constitutive model. The formulas for surface-based cohesive behaviour closely resemble those used for cohesive elements exhibiting traction-separation behaviour [37]. Traction-separation laws were applied to characterise the response of joints in failure modes 1, 2, or 3, representing failure in tension and shear. Initially, the joint behaved linearly, and the K_n, K_s, and K_t values are the stiffnesses of the joint. The plastic response of the joint interfaces begins to reach the peak traction value. Moreover, t_n and t_t are the normal and shear stresses, respectively, and d_n and d_s respectively represent the separations in the normal and shear stresses (Figure 15). The nominal stress criterion was

used to define damage initiation. The tensile strength of the joint was assumed to be 0.173 MPa. Furthermore, the Mohr–Coulomb shear sliding characteristics were characterised by a coefficient of friction set at 0.66 to simulate post-joint failure behaviour, indicating that the joint will experience sliding if the shear stress surpasses the critical shear stress. In the Mohr–Coulomb behaviour, the cohesion coefficient was assumed to be zero, and the pressure was multiplied by the coefficient of friction (0.66). The fracture energies of the joints were derived from the experimental data. The Mod-1 and Mod-2 fracture energies were 0.10 N/mm and 0.18 N/mm, respectively. As indicated in the Abaqus manual [37], the surface-based cohesive behaviour formulae were very similar to those used for cohesive elements with traction-separation behaviour; accordingly, it was assumed that the fracture energies (the areas under the traction-separation graph) were the same. The mixed-mode behaviour in the computational model was captured using the Benzeggagh–Kenane rule. As mentioned in a previous investigation [38], when there is no distinction in the critical fracture energies between the second- and third-mode shear failures, the Benzeggagh–Kenane rule is the most appropriate choice for capturing the critical mixed-mode fracture energy. The same study suggested the use of a Benzeggagh–Kenane exponent value of two for brittle joints [38].

In a previous study, the fracture energies of flexible joints were compared with those of mortar joints; this comparison showed that the polymer joints undergo extensive and more prominent damage and have higher total fracture energies. The polymer joint-fracture energy values were obtained from this study and were set to 4.22 N/mm and 10.93 N/mm for first and second-mode behaviour, respectively [38].
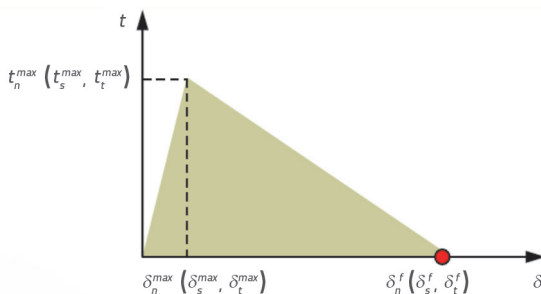
Figure 15. Traction-separation behaviour [37]

2.3.7. Model analysis

The C3D8R element was used for all materials in the model, except for the rebars. The C3D8R element is an 8-node linear element with reduced integration and hourglass control (Figure 16). A two-node linear beam element (B31) was used for the rebar. For the loading of the frame, explicit dynamic analysis was used; in Abaqus, this type of analysis is more suited for non-linear quasi-static problems involving contact.
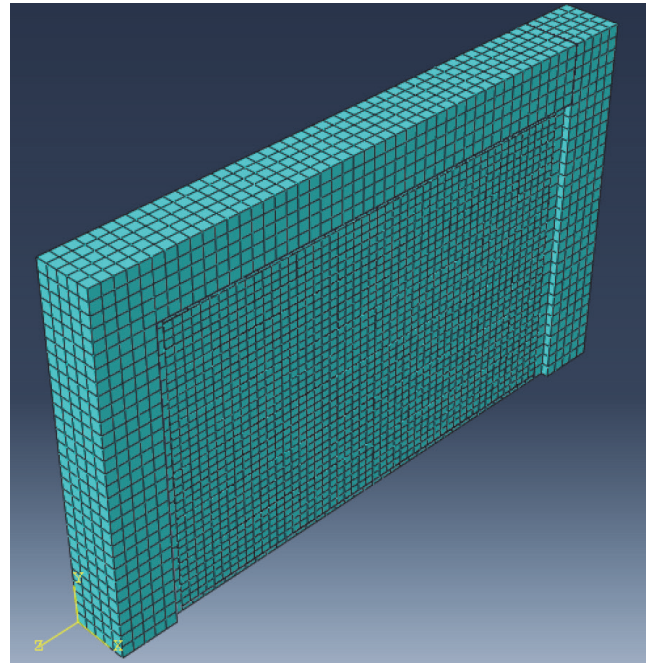
Figure 16. Model mesh

To solve the equation of motion, the central difference method was used instead of the Newton–Raphson method. A major advantage of this approach is its low-computational cost. This is because the stiffness, mass, and damping matrices were not created at each iteration. Instead, the displacements in steps I + 1 were determined by utilising the displacements in steps I and I - 1. The computational power requirement determines the internal forces of the elements [27].

Certain conditions must be considered for a successful explicit analysis if it will be used to simulate quasi-static loading because in these situations, static loading is transformed into dynamic loading. If the inertial forces are maintained below a certain limit, the problem can be regarded as static. This determination can be made post-analysis by examining the ratio of the kinetic to the total internal energy. If this ratio was less than or equal to 0.10, the analysis was categorised as quasi-static loading [27]. For all the analyses, a lateral displacement loading of 60 mm was applied to the frames at a loading time of 6 s.

3. Results

3.1. Cyclic test results of bare frame

There was no fracture in the RC frame members during the hysteretic cycles of 5 kN (0.13 mm displacement), 7.5 kN (0.22 mm displacement), and 10 kN (0.50 mm displacement). At approximately 15 kN (0.9 mm), microcracks appeared in the region where the hydraulic actuator touched the frame. In the cycles of 45 kN, (8 mm displacement), it was possible to observe the beginning of flexural damage at the bottom
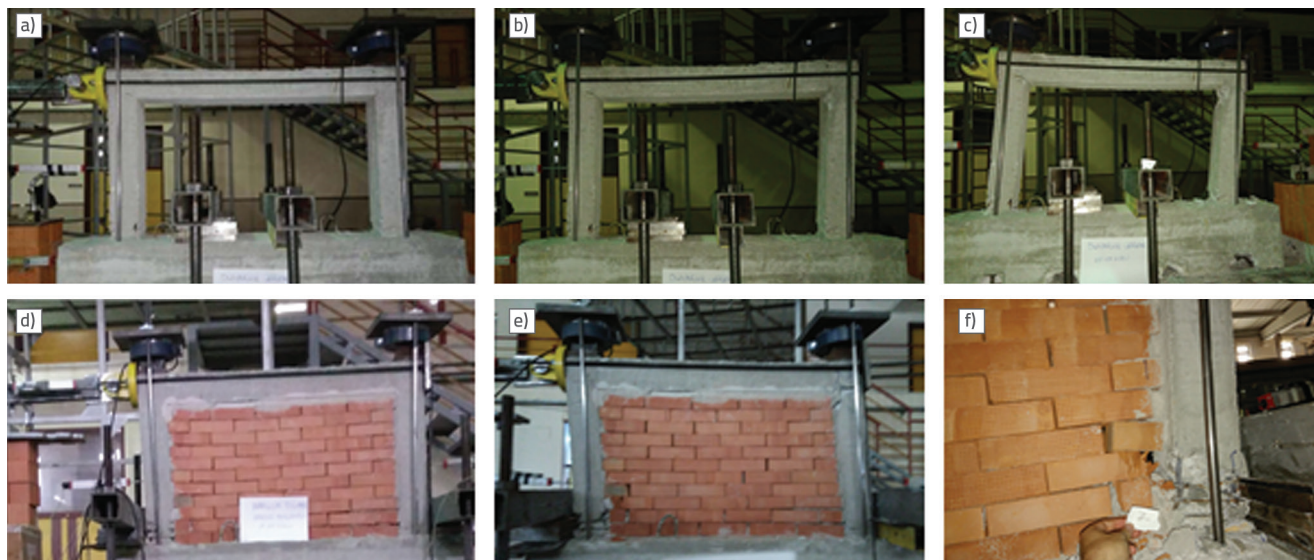
Figure 17. Damage evolutions: a) Bare frame at the beginning; b) Bare frame at the maximum load (drift ratio of 0.037); c) Bare frame at the maximum displacement (drift ratio of 0.08); d) Dry stack masonry infilled frame at the beginning; e) Dry stack masonry infilled frame at the maximum load (drift ratio of 0.04); f) Dry-stack masonry infilled frame at the maximum displacement (drift ratio of 0.09)

parts of the columns and cracks in the column-beam bonding zone. In the 55 kN (13 mm displacement) cycles, shear cracks were observed in the columns, and the damage increased in the column-beam bonding zone. The maximum load was 63 kN (28 mm displacement). The initial stiffness of the frame can be considered as 12259.09 N/mm if a load value of 26970 N is regarded as the starting point of frame yielding. The damage situation at different loading stages is shown in Figure 17.

3.2. Cyclic test results of dry stack masonry infilled frame with mortar joint

In this experiment, column damage occurred in the beam-bonding zone. The first microcrack was observed at the upper mortar joint of the infill wall. In cycles of 35 kN (4.5 mm displacement), the infill wall started to lose contact with the frame. In the 40 kN cycles (6 mm displacement), cracks occurred between the column and the beam's bonding zone. In the maximum load cycle of 65.1 kN (displacement of 30 mm), diagonal shear cracks appeared in the top and bottom zones of each column, where they bonded with the beam and foundation. The infill did not fail in the out-of-plane direction even if there was no restraint during the experiment. The infill wall exhibited no serious damage, and most bricks were reusable if demounted after the experiments. The frame's states at the various loading stages are shown in Figure 17.

After the failure, a large displacement of 80 mm was attempted for demonstration. The cracks at a large displacement of 80 mm are shown in Figure 18.

Figure 18. Frame with dry-stack masonry infill and mortar joint with a large displacement of 80 mm (drift ratio of 0.1)

3.3. Cyclic test results of dry stack masonry infilled frame with a polymer joint

In this experiment, no serious damage was observed for loads lower than 30–35 kN (5–5.5 mm displacement). During the 40 kN loading cycles (7.5 mm displacement), flexural cracks started to occur at the point where the columns bonded to the foundation. During the 50 kN loading cycles (11 mm displacement), increased damage was visible in the column-beam bonding zone. Under the maximum loading conditions at 65 kN (52 mm displacement), diagonal shear cracks were observed at the top of the columns at the sites at which they bonded to the beams (Figure 19). When the lateral loading increased to 65 mm, the infill wall did not lose contact with the frame, indicating that the polymer bond was much stronger

than the mortar bond. Minimum damage was inflicted to the wall bricks. The frame's states at the various loading stages are shown in Figure 20. The initial stiffness of the frame can be considered to be 10032.14 N/mm if a load value of 28090 N is regarded as the starting point of frame yielding.
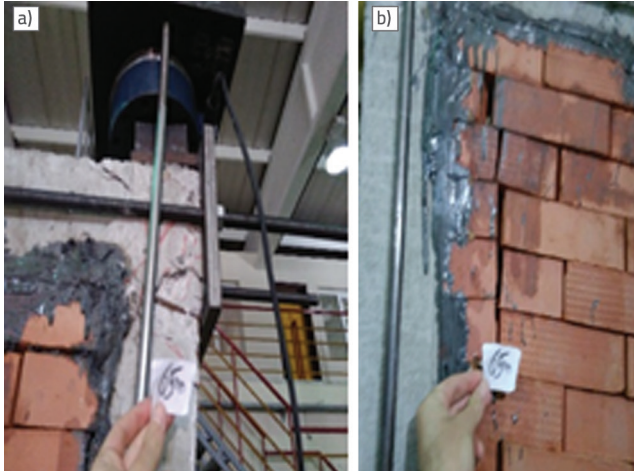
Figure 19. a) Damage in column-beam joint (drift ratio of 0.08); b) Separation in the mortarless wall (drift ratio of 0.08)

3.4. Cyclic test results of the frame with traditional infill

No damage was observed in the infill wall in this experiment for loads up to 50 kN (3.88 mm displacement). Micro-cracks occurred in the column–beam and column–foundation bonding zones, as expected, in line with previous experiments. Displacements were controlled at loads greater than 70 kN (displacement of 13.62 mm) to continue lateral loading. At the lateral loading of 20 mm, cracks occurred in the infill wall. At the lateral loading of 30 mm, the upper part of the infill wall collapsed in the out-of-plane direction, causing a short-column effect. Figure 21 shows the damaged frame at the maximum displacement. At a displacement of 30 mm, diagonal shear cracks were visible in the columns, as expected. Loading was completed at a depth of 60 mm. The initial stiffness of the frame was considered to be 17678.11 N/mm if the load value of 41190 N was regarded as the starting point of frame yielding. A comparison of all the hysteretic loops of the frames is shown in Figure 22. A comparison of all the envelope curves of the hysteresis loops is shown in Figure 23.

Figure 21. Damaged frame with conventional infill at the maximum displacement (drift ratio of 0.08)
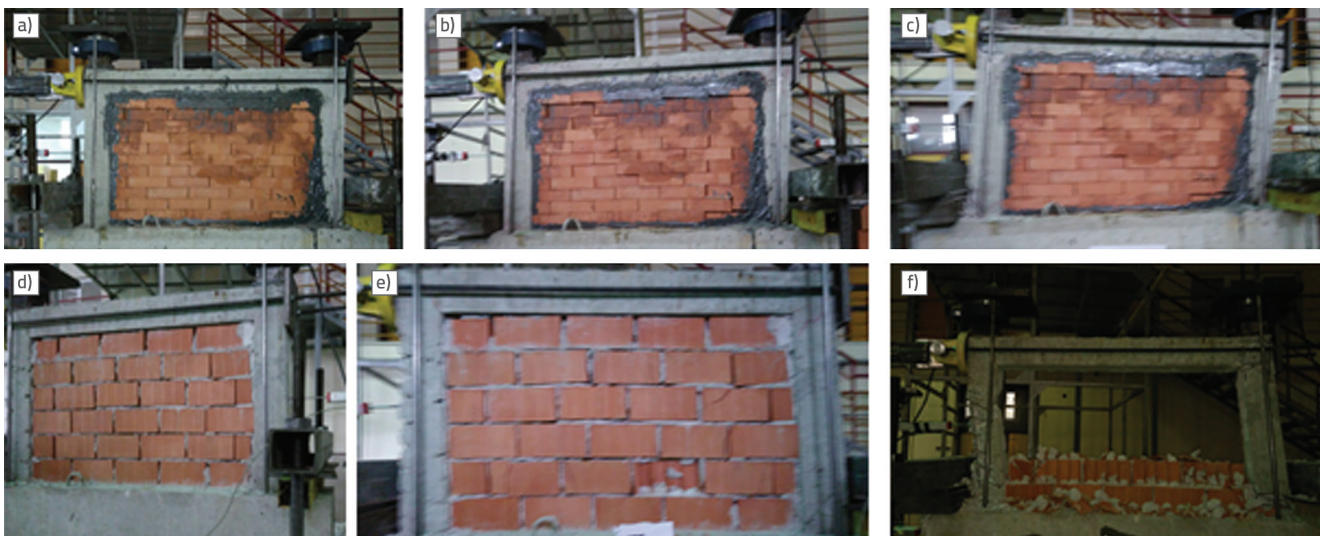
Figure 20. a. Dry-stack masonry and polymer at the beginning; b) Dry-stack masonry and polymer at the maximum load (drift ratio of 0.07); c) Dry stack masonry and polymer at the maximum displacement (drift ratio of 0.086); d) Traditional frame at the beginning; e)Traditional frame at the maximum load (drift ratio of 0.018); f) Traditional frame at the maximum displacement (drift ratio of 0.08)
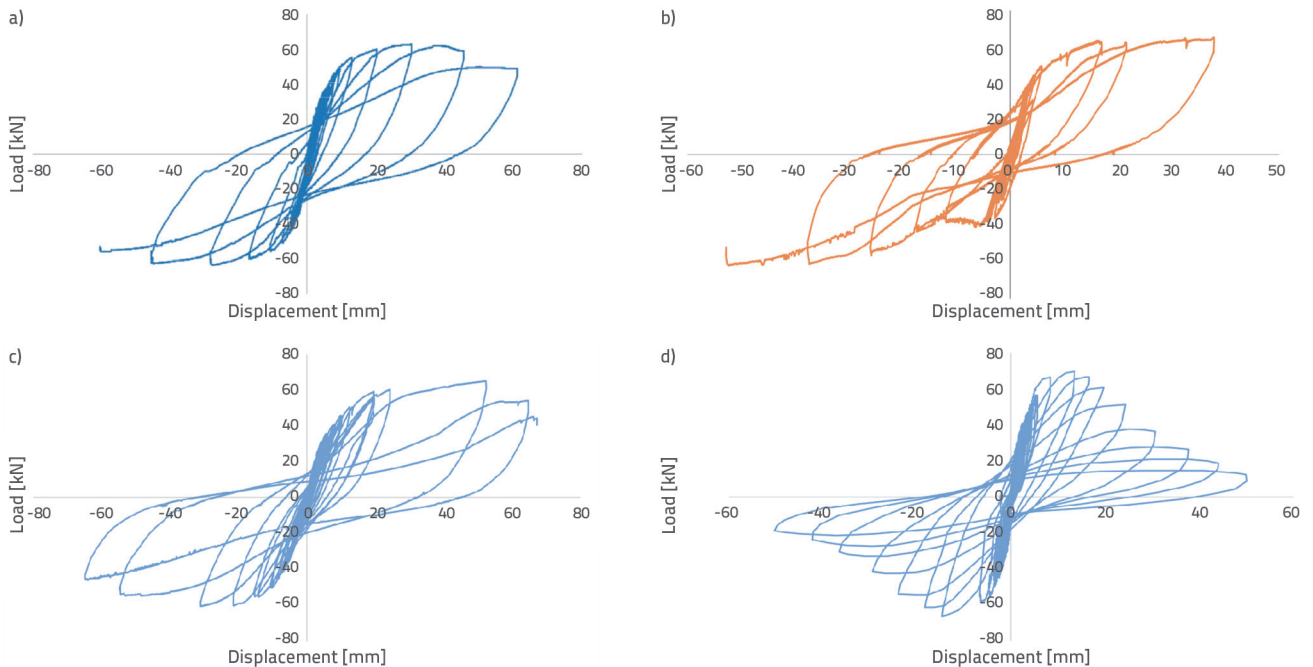
Figure 22. a) Hysteretic loops of a bare frame; b) Hysteretic loops of frame with dry-stack masonry and mortar joint; c) Hysteretic loops of frame with dry-stack masonry and polymer joint; d) Hysteretic loops of the traditional frame
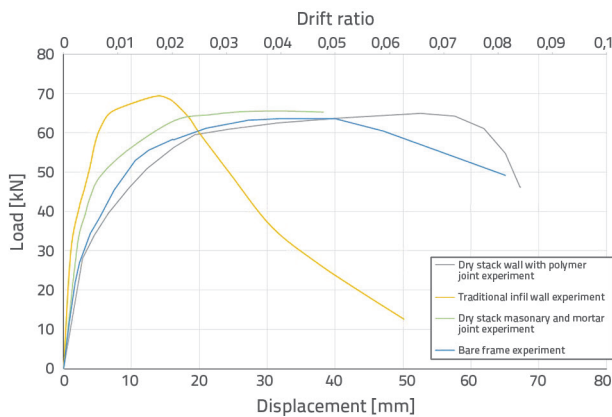
Figure 23. Comparison of envelopes obtained from experiments

Damage to frames can be classified using the European Macroseismic Scale 98. In the cyclic tests, all specimens were forced to have large lateral drifts (up to 0.08); thus, shear cracks were visible in the columns, and spalling of the concrete cover was detected. In addition, the buckling of the reinforced rods and failure of the traditional infill wall were observed. However, the columns failed and the storey did not collapse. Thus, the grade of the damage was in the range of 3–4 at the end of the loading level, as shown in Figures 27–29.

Figure 24 shows the normalised graph of envelopes obtained from the experiments. For normalisation, the corresponding relationships of the other frames were normalised to the behaviour of the bare frame. The load levels based on the drift ratios are listed in Table 2.

Table 2. Load level comparison according to the drift ratio

Drift ratio (exp.)	Load in bare frame [kN]	Load in frame with dry stack masonry and mortar [kN]	Load in frame with dry stack masonry and polymer [kN]	Load in frame with traditional infill [kN]
0.01	46.785	52.41	41.47	65.7
0.02	58.288	63.22	54.612	68.7
0.03	62.15	64.71	60.4	55
0.04	63.6	65.5	62.164	36.17
0.05	63.6	65.32	63.30	26.74
0.06	59.88	61.44	64.18	18.8
0.07	54.88	61.4	64.95	11.68
0.08	49.88	–	62.47	–
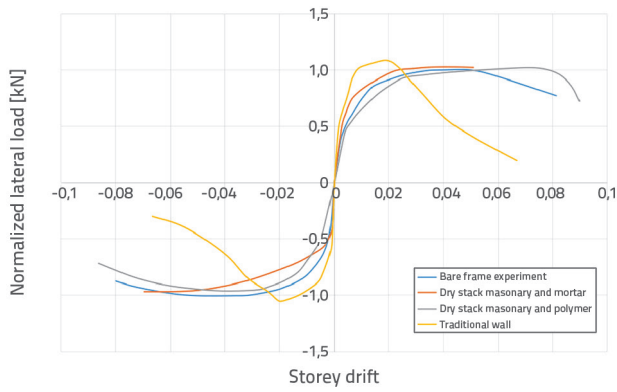
Figure 24. Normalised graph of envelopes from the experiments

3.5. Computational analysis results

3.5.1. Bare frame results

In the computational model, the analysis revealed the force–displacement relations of the frame, energy graphs, and stress values. The bare frame without infill withstood 57.1 kN. The initial stiffness of the frame can be considered to be 15230 N/mm if a load value of 32744 N is regarded the starting point of frame yielding. The yield displacement was observed as 4.55 mm. The displacement ductility was considered to be equal to 13.18. The lateral-load–displacement curves obtained after the analysis are shown in Figures 27–29. The von Mises stresses on the bare frame are shown in Figure 25.
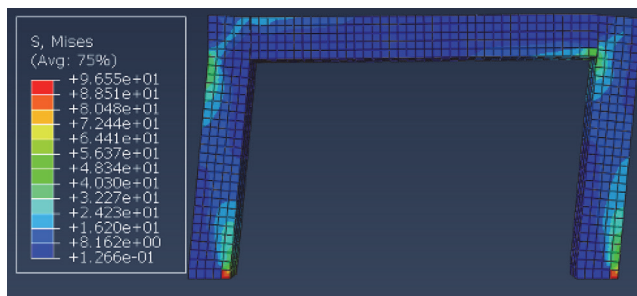
Figure 25. Von Mises stresses in a bare frame in concrete

Figure 26. Damaged frame

Figure 26 shows the damaged frame at the maximum displacement. In the damaged zones, von Mises stresses varied between 56.37 MPa and 96.5 MPa. The stresses exceeded the strength of the concrete.
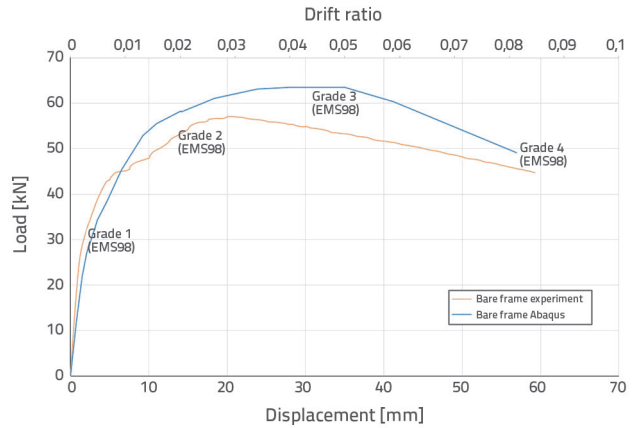
Figure 27. Comparison of numerical analysis and experimental backbone curves of bare frames
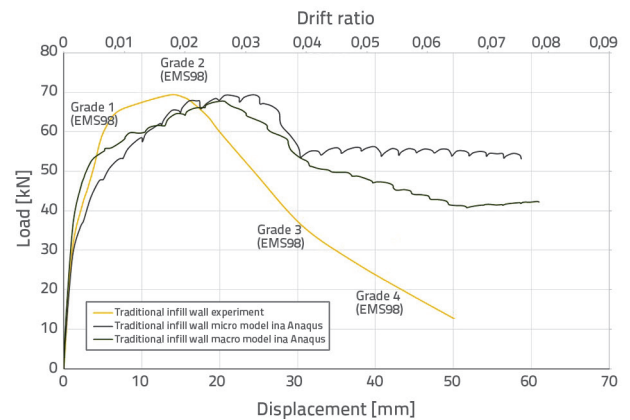
Figure 28. Comparison of numerical analysis and experimental backbone curves of frames with traditional infill
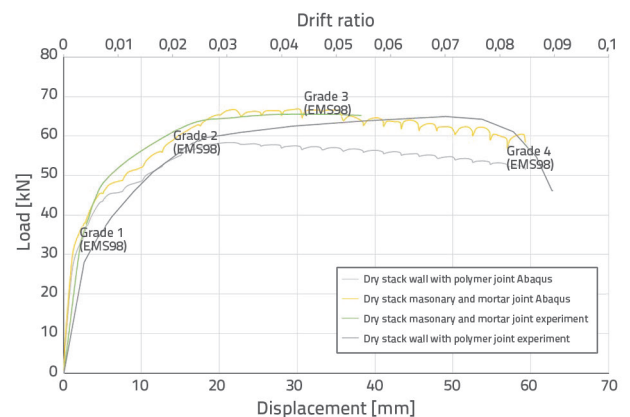
Figure 29. Comparison of numerical analysis and experimental backbone curves of frames with dry stack masonry
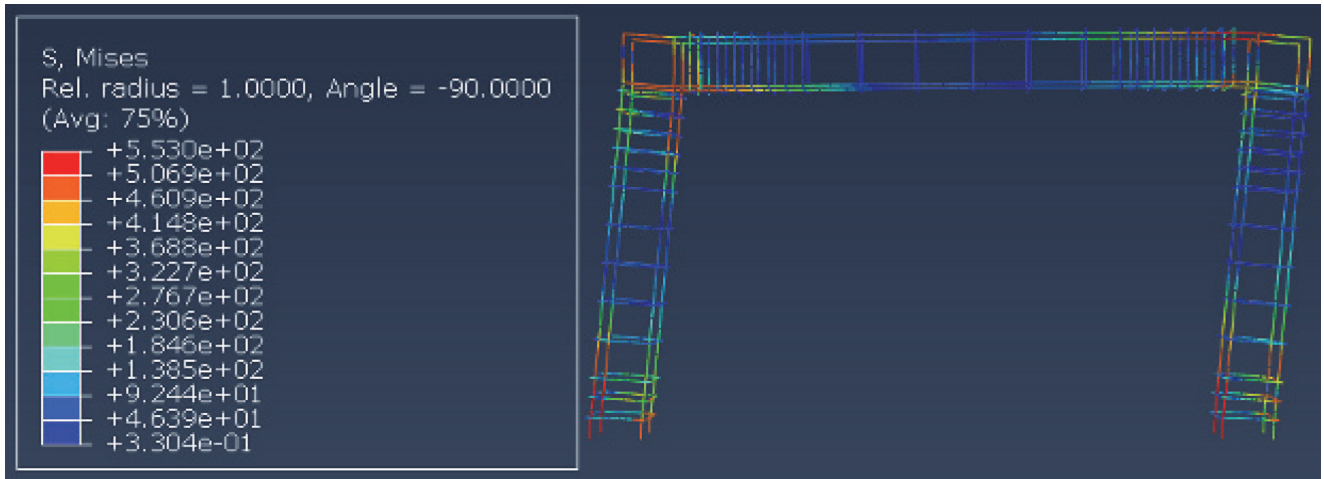
Figure 30. Von Mises stress distribution in rebar

There was a small discrepancy between the computational model curve and the experimental backbone curve. The maximum stress value in the rebars reached 553 MPa as shown in Figure 30. This indicates considerable yielding before the collapse. This value is consistent when the damaged zones in the experiments are considered.

3.5.2. Frame with dry stack masonry and mortar joint

The frame with the infill and mortar binder between the wall and frame withstood 67 kN. If the lateral displacement of 2.15 mm is considered as the starting point of the non-linear stage, the initial stiffness of the frame is 16816.44 N/mm. Therefore, a design involving mortarless masonry can be considered as a combination of a weak compression strut and higher viscous damping. Based on the initial stiffness, this suggests the benefits of an equivalent frame with a compressive strut for the building design. Mortarless masonry had no negative effect on displacement ductility. The energy graphs show low-kinetic energy/total internal energy values. Figure 31 shows an energy graph for the frame with dry-stack masonry and mortar joints. The other frames were also evaluated. This indicates that the analysis can be considered quasi-static. The frictional energy dissipation of the assembly is illustrated in Fig. 32.
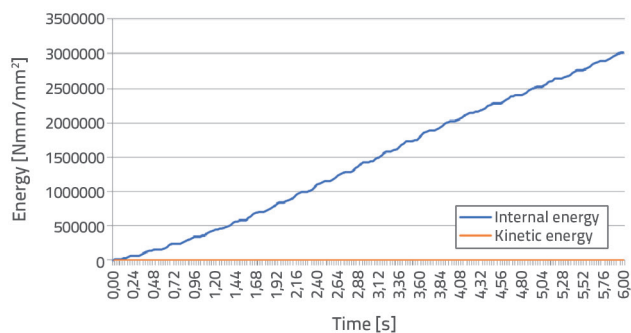
Figure 31. Comparison of kinetic energy and internal energy of the frame with dry-stack masonry and mortar joints
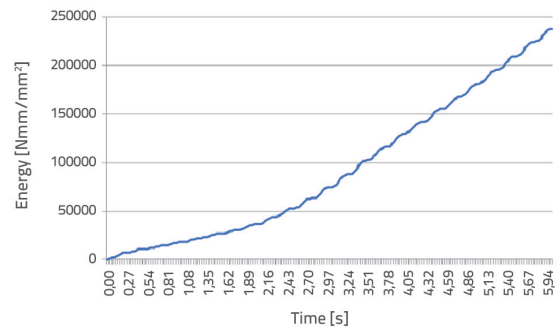
Figure 32. Frictional energy dissipation of the frame with dry-stack masonry and mortar joints

During the experiments, the dry stack bricks were not damaged. The von Mises stresses in the damaged zones of the wall (the frame is not shown) were in the range of 3.82–6.53 MPa as shown in Figure 35. The absolute principal stresses (measured in MPa) on the wall are shown in Figure 36.

The mortarless walls increased the lateral load capacity of the bare frame by 17 %. In a previous study where mortarless semi-interlocking concrete blocks were used as the infill [10], the increase was approximately 1.4 times. This may be related to the fact that in a previous study, the vertical pressure was higher on mortarless blocks owing to the loading conditions.
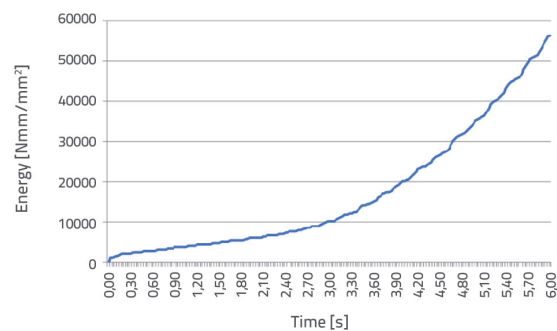
Figure 33. Frictional energy dissipation of frame with dry-stack masonry and polymer joints

3.5.3. Frame with dry stack masonry and polymer joint

In that analysis, the load of 58.36 kN was withstood by the frame with infill and with polymer adhesive binder between the wall and frame. If a displacement of 2.14 mm is considered the yield displacement, the initial stiffness is 15,512 N/mm, which is almost identical to that of the bare frame. This means that mortarless masonry has no negative effect on the yield displacement and displacement ductility of the structure. When polymer bonds are used, there are minor differences in the periods of the structures. The frictional energy dissipation of the assembly is illustrated in Figure 33. This energy was used to calculate the equivalent damping ratio. Regions with high von Mises stresses were consistent with the regions showing the greatest damage in the experiments (Figure 34). The von Mises stresses in the damaged zones of the wall were in the range of 1.21–3.63 MPa, as shown in Figure 37. This indicates that the polymer binder decreased the stress on the wall. The absolute principal stresses (measured in MPa) decreased at the wall when the polymer binder was used, as shown in Figure 38.

3.5.4. Frame with traditional infill

A frame with traditional infill was modelled using macro- and micro-approaches. The macro approach expressed by Eqs. 7–9, was based on the Eurocode and was adopted from a previous study [40]. The compressive strengths of the brick and mortar were 3.56 MPa and 5 MPa, respectively. In a previous study, the maximum strain for masonry was proposed to be 0.0088; accordingly, this strain was used for masonry in this study. The calculated modulus of elasticity of the masonry was 1012.24 MPa using Eq. 9 [41]. The symbols t_H, t_e, E_H, E_e, k, and E_d are the thickness of the mortar, thickness of the brick, modulus of elasticity of the mortar, modulus of elasticity of the brick, coefficient related to adherence, and
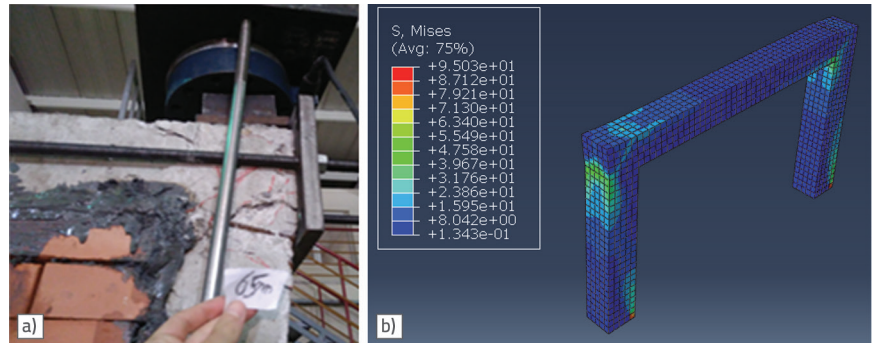
Figure 34. a) Damaged zones in experiments; b) Von Mises stress in the frame with polymer
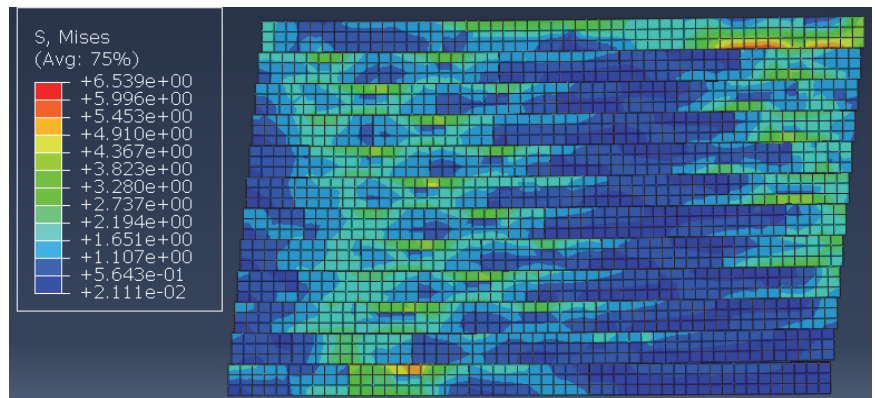
Figure 35. Dry-stack wall von Mises stresses in the frame with mortar
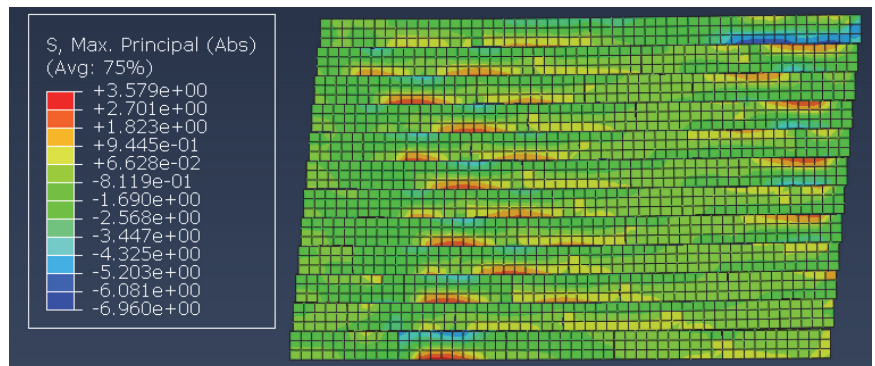
Figure 36. Dry stack wall's maximum absolute principal stresses in the frame with mortar
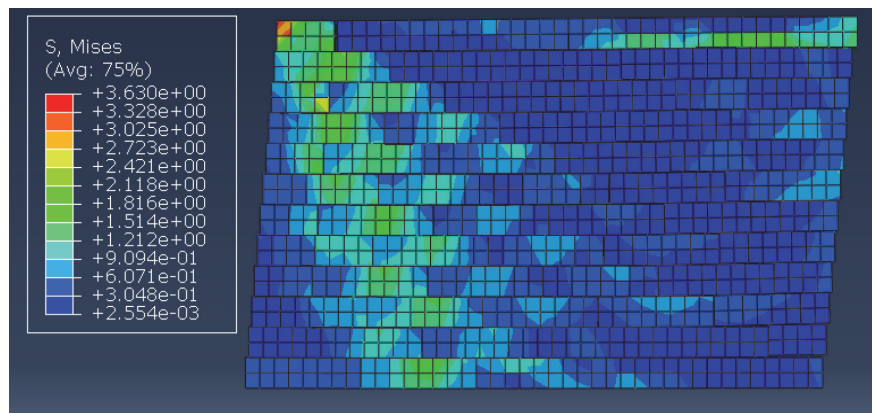
Figure 37. Dry-stack wall von Mises stresses in a frame with polymer
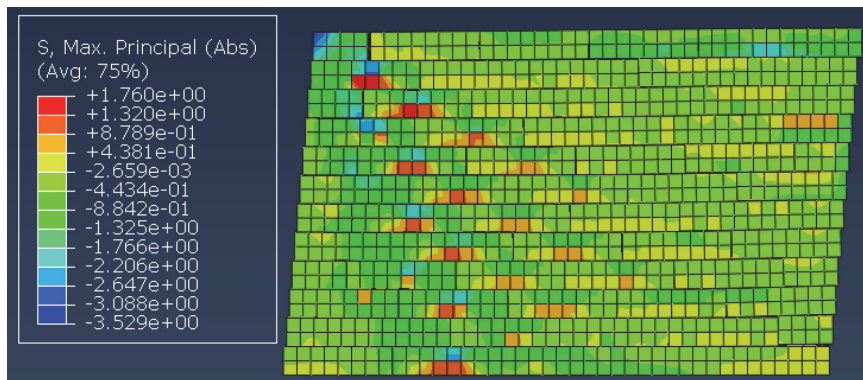
Figure 38. Dry stack wall's maximum absolute principal stresses in frames with polymers
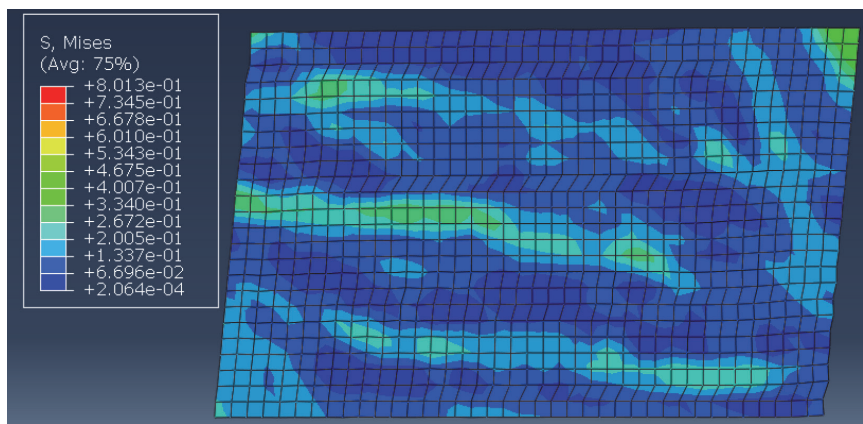
Figure 39. Traditional wall von Miss stresses in macro modelling
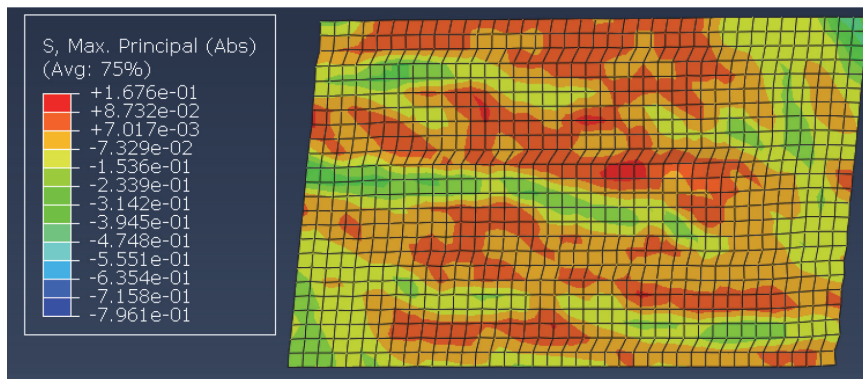
Figure 40. Traditional wall's maximum absolute principal stresses in macro modelling

modulus of elasticity of the masonry, respectively. The wall was modelled using a macro model, and a mortar layer was modelled between the wall and frame using the same traction separation laws as those used in previous analyses. In the CDP model used for the macro modeling of the masonry, the dilation angle and eccentricity were assumed to be one, and the viscosity parameter was assumed to be 0.004. These values were used in a previous study which reported similar results [42]. The wall thickness in the macro model was 100 mm. In micro modelling, the brick, mortar, and the mortar interfaces were modelled separately. The compressive strength was taken as 3.56 MPa and its modulus of elasticity was 1111 MPa.

$$f_{ckmax} = 0.4 \times 3.56^{0.75} \times 5^{0.25} = 1.57 \, \text{MPa} \qquad (7)$$

$$f_{cktensile} = 0.4 \times 0.9^{0.75} \times 0.257^{0.25} = 0.26 \, \text{MPa} \qquad (8)$$

$$E_d = [(t_t + t_h)/((t_t / E_t) + t_h / E_h))] \times k \qquad (9)$$

The frame with traditional infill withstood a maximum load of 69 kN. In macro modelling, the initial stiffness of the frame was 21618.60 N/mm, which was higher than the micro model analysis which yielded a value of 16850 N/mm. In the experiments, the upper part of the wall failed in the out-of-plane direction, but in the computational model, in which loading was in the in-plane direction, no such failure was observed. These findings may explain the difference between the computational results and the experimental backbone curve for

Table 3. Comparison of experimental and computational results

Label	Maximum drift at failure (Experimental)	Max. load (Experimental) [kN]	Initial stiffness (Experimental) [N/mm]	Max. drift (Computational model)	Maximum load (Computational model) [kN]	Initial stifness (Computational model) [N/mm]
Bare frame	0.08	63	12259.09	0.08	57.1	15230
Dry stack panel with mortars	0.08	65.09 (3 %)	15348.57 (25 %)	0.08	67 (17 %)	16816.44 (10 %)
Dry stack panel with polymer	0.086	65 (3 %)	10032.14 (-)	0.08	58.36 (2 %)	15512 (1 %)
Traditional frame	0.06	70 (11 %)	17678.11 (44 %)	0.078	69 (20 %)	21618.6 (41 %)

displacements greater than 30 mm. Figure 39 shows the Von Mises stresses (measured in MPa). The maximum absolute principal stresses (measured in MPa) are presented in Fig. 40. A comparison of all the results in terms of lateral drifts, initial stiffnesses, and maximum loads is presented in Table 3. Increments with respect to the bare frame results are provided in parentheses.

4. Conclusions

The numerical analyses conducted herein showed that dry-stack masonry increased the energy dissipation of the frame owing to friction. The binder between the wall and the frame changed the behaviour. In the computational model, the maximum load of the frame with dry-stack masonry and mortar was 1.17 times the maximum load of the bare frame. The frame is expected to withstand increased lateral loads if the specimens were designed to have a strong column-weak beam mechanism owing to the equivalent compressive strut behaviour. The traditional infill wall increased the stiffness of the frame by 1.42 times whereas the dry-stack masonry with mortar increased the stiffness by 10 % only when the mortar was used in the computational model. When a polymer binder was used with dry-stack masonry, no increase occurred in the computational model.

In the experiments, there was a 3 % difference between the maximum loads of the dry-stack masonry and bare frame. The frame with traditional infill had more lateral rigidity (1.44 times that of the bare frame). A dry stack wall with mortar between the wall and frame increased the lateral rigidity by 1.25 times. The frame with the polymer exhibited a behaviour similar to that of the bare frame, especially with respect to the initial stiffness. This can increase the period of the structure and decrease spectral acceleration. Thus, earthquake loading can decrease. This phenomenon shows that structures may be more durable if a polymer adhesive is used in conjunction with dry-stack masonry and also reveals considerable potential for decreasing earthquake loads. In addition, dry-stack masonry can eliminate the problems caused by stiffness differences between stories. Another aspect is the traditional out-of-plane failure of the infill wall, which results in a more brittle behaviour. The traditional infilled frame failed at a drift of 0.06, whereas the mortarless masonry exhibited no damage even at large drifts (of the order of 0.08). As expected, mortarless masonry had no negative effect on displacement ductility. In addition, the polymer binder exhibited more prominent ductile behaviour after the peak loads. In the design of structures, dry-stack masonry decreases the stiffness of the structure; however, this can lead to higher storey drifts which must be controlled. Based on the initial stiffness, an equivalent frame with a compressive strut can be beneficial for the building's design.

A mortar's lower deformation capacity results in higher stress concentrations when a wall deforms in the vertical direction, whereas the polymer decreases the stress concentrations because of its higher elasticity; however, lower frictional dissipation occurs. Thus, these two methods have different advantages and disadvantages, and the appropriate method should be chosen. TSC 2018 proposed a flexible bond between a traditional wall and frame to prevent problems caused by infill wall-frame interaction and eliminate the problem of unreliable behaviour of traditional infills in high-lateral drifts. The overall results show that when used with polymer injection, mortarless masonry is more effective in providing more lateral drift to the structure.

These results highlight the potential of dry-stack masonry as an alternative approach for the design and seismic retrofitting of existing structures.

REFERENCES

[1] Yıldırım, S., Aşık, G., Erkus, B., Yetimoğlu, Y., Tonguç, Y., Mualla, I.: Retrofit of a reinforced concrete building with friction dampers, Second European Conference on Earthquake Engineering and Seismology, İstanbul, pp. 25-29, 2014

[2] Nikam, S., Wagholikar, S., Patil, G.: Seismic energy dissipation of a building using friction damper, International Journal of Innovative Technology and Exploring Engineering, 3 (2014) 10, pp. 2278-3075

[3] Li, H., Li, G., Wang, S.: Study and application of metallic yielding energy dissipation devices in buildings, 10th National Conference on Earthquake Engineering, Alaska, 2014.

[4] Nicola, T., Leandro, C., Guido, C., Enrico, S.: Masonry infilled frame structures: State of art review of numerical modelling, Earthquakes and Structures, 8 (2015), pp. 225-251, http://dx.doi.org/10.12989/eas.2015.8.1.895

[5] Lin, K., Totoev, Y.Z., Guo, H.L.T.: In-plane behaviour of a reinforcement concrete frame with a dry stack masonry panel, Materials, 9 (2016), Paper 108. https://doi.org/10.3390/ma9020108

[6] Totoev, Y.: Design procedure for semi-interlocking masonry, Journal of Civil Engineering and Architecture, 9 (2015), pp. 517-525, https://doi.org/10.17265/1934-7359/2015.05.003

[7] Hossain, A., Totoev, Y., Masia, M.J.: Energy dissipation of framed semi-interlocking masonry panel under large displacement, 10th Australian Masonry Conference, Sydney, pp. 344-355, 2018.

[8] Totoev, Y.Z., Lin, K.: Frictional energy dissipation and damping capacity of framed semi-interlocking masonry infill, 15th International Brick and Block Masonry Conference, Florianopolis, Brazil, 2012.

[9] Totoev, Y., Harty, A.: Semi-interlocking masonry as infill wall system for earthquake resistant buildings, The Journal of Engineering Research, 13 (2016) 1, pp. 33-41, http://dx.doi.org/10.24200/tjer.vol13iss1pp33-41

[10] Sanada, Y., Yamauchi, N., Takahashi, E., Nakano, Y., Nakamura, Y.: Interlocking block infill capable of resisting out-of-plane loads. The 14th World Conference on Earthquake Engineering, Beijing, 2008.

[11] Mısır, S., Özcelik, Ö., Girgin, S., Kahraman, S.: Experimental work on seismic behaviour of various types of masonry infilled RC frames, Structural Engineering and Mechanics, 44 (2012) 6, pp. 763-774, http://doi.org/10.12989/sem.2012.44.6.763

[12] Milanesi, R.R., Totoev, Y., Morandi, P., Rossi, A., Magenes, G.: Estimation of basic dynamic characteristics of liable masonry infills with horizontal sliding joints from in-plane test results, 7th Eccomas Thematic Conference on Computational Methods in Structural Dynamics and Earthquake Engineering, Crete, pp. 2543-2564, 2019.

[13] Shendkar, M., Ramancharla, K.P.: Response reduction factor of RC frame structures with semi-interlocked masonry and unreinforced masonry infill, Indian Concrete Institute (ICI) Journal, 1 (2018), pp. 24-28.

[14] Kwiecien, A.: Highly deformable polymers for repair and strengthening of cracked masonry structures International Journal of Engineering Technology, 2 (2013) 1, pp. 182-196, http://dx.doi.org/10.5176/2251-3701_2.1.53

[15] Kwiecien, A., de Felice, G., Oliveira, D.V., Zajac, B., Bellini, A., De Santis, S., Ghiassi, B., Lignola, G.P., Lourenço, P.B., Mazzotti, C., Prota, A.: Repair of composite to masonry bond using flexible matrix, Materials and Structures, 49 (2016) 7, pp. 2563-2580, https://doi.org/10.1617/s11527-015-0668-5

[16] Kwiecien, A.: Shear bond of composites to brick applied highly deformable, in relation to resin epoxy interface materials, Materials and Structures, 47 (2014), pp. 2005-2020, https://doi.org/10.1617/s11527-014-0363-y

[17] Kwiecien, A., Gams, M., Zajac, B.: Numerical modelling of flexible polymers as the adhesive for frps, The 12th International Symposium on Fibre Reinforced Polymers as The Adhesive for FRPs, Nanjing, 2015.

[18] Akyıldız, A.T., Kwiecien, A., Zajac, B.,Triller, P., Bohinc, U., Rousakis, T., Viskovic, A.: Preliminary in-plane shear tests of infills protected by PUFJ interfaces, Brick and Block Masonry (2020), Taylor and Francis Group, London, pp. 968-975

[19] Rousakis, T., Papadouli, E., Sapalidis, A., Vanian, V., İlki, A., Halici, O.F., Kwieicien, A., Zajac, B., Hojyds, L., Krajewski, P., Tekieli, M., Akyıldız, A.T., Viskovic, A., Rizzo, F., Gams, M., Triller, P., Ghiassi, B., Colla, C., Benedetti, A., Rakicevic, Z., Bogdanovic, A., Manojlovski, F., Saklarovski, A.: Flexible Joints between RC frames and masonry infill for improved seismic performance–shake table tests, Brick and Block Masonry, (2020), pp. 499-507

[20] Kwiecien, A., Rakicevic, Z., Bogdanovic, A., Manojlovski, F., Poposka, A., Shoklarovski, A., Rousakis, T., İlki, A., Gams, M., Viskovic, A.: PUFJ and FRPU earthquake protection of infills tested in resonance., 1st Croatian Conference on Earthquake Engineering, Zagreb, Croatia, pp. 465-475, 2021.

[21] Abaqus 3D Experience R2017, Dassault Systems SIMULIA Corp. 1301 Atwood Avenue, Suite 101 W Johnston, RI 02919, USA

[22] Al-Shaikh, I., Falah, N.: Numerical analysis of masonry infilled RC frames, Journal of Science and Technology, 19 (2014) 2, pp. 21-38

[23] Vermeltfoort, A.: Brick Mortar Interaction in Masonry Under Compression, Eindhoven University of Technology, Eindhoven, 2005.

[24] Van Noort, J.R.: Computational Modelling of Masonry Structures, Delft University of Technology, Delft, 2012.

[25] TSC-18 (2018) Specifications for buildings to be built in seismic areas, Turkish Building Earthquake Code. Ministry of Public Works and Settlement, Ankara.

[26] Birdal, F.: Analytical modelling and experimental investigation of RC structures, Kayseri University, Kayseri, 2015.

[27] Demir, C.: Seismic Behaviour of Historical Stone Masonry, Istanbul Technical University, İstanbul, 2012.

[28] Koman, H., Nohutcu, H.: Numerical analysis of reinforced concrete frame with dry stack masonry infill, Niğde Ömer Halisdemir Üniversity Journal of Engineering Sciences, 10 (2021) 1, pp. 266-275, https://doi.org/10.28948/ngumuh.785286

[29] Unal Engineering Bornova. https://unalmuhendislik.com/en/

[39] OPKON Optic Electronic Control Sytems, Bayrampasa, İstanbul. https://www.opkon.com.tr/en/contact

[31] Sayed, A.M., Javed, M., Alam, B.: Similitude analysis of concrete scaled bridge columns for quasi-static and free vibration testing, Journal of Mechanical and Civil Engineering, 3 (2012) 6, pp. 42-48

[32] Santos, C.F.R., Alvarenga, R.C.S.S., Riberio, J.C.L., Castro, L.O., Silva, R.M., Santos, A.A.R., Nalon, G.H.: Numerical and experimental evaluation of masonry prisms by finite element method, Ibracon Structure and Materials Journal, 10 (2017) 2, pp. 477-508, https://doi.org/10.1590/S1983-41952017000200010

[33] Inculet, V.: Nonlinear Analysis of Earthquake-induced Vibrations, Aalborg University, School of Engineering and Science, Denmark, 2016.

[34] Obaidat, Y.T.: Structural Retrofitting of Concrete Beams Using FRP. Lund University, Lund, 2011.

[35] Erkek, S.: Kauçuk Kapı Stoperinin Hiperelastik ve Viskoelastik Modellenmesi ve Sonlu Elemanlar Yöntemi ile Analizi, Uludağ University, Bursa, 2016.

[36] Ksiel, P.: Model Approach for Polymer Flexible Joints in Precast Element Joints for Concrete Pavements, Krakow University of Technology, Krakow, 2018.

[37] Dassault Systems Simula Abaqus, Modelling Fracture and Failure, Lecture 6

[38] Abdulla, K.F., Cunningham, L.S., Gillie, M.: Simulating masonry behaviour using a simplified micro model approach, Engineering Structures, 151 (2017), pp. 349-365, https://doi.org/10.1016/j.engstruct.2017.08.021

[39] Viskovic, A., Zuccarino, L., Kwiecien, A., Zajac, B., Gams, M.: Quick seismic protection of weak masonry infilling in filled frame structures using flexible joints, Key Engineering Materials, 747 (2017), pp. 628-637, https://doi.org/10.4028/www.scientific.net/KEM.747.628

[40] Doğan, H.N.A.: Yığma Duvarların Mikro ve Makro Modelleme Teknikleri ile Lineer Olmayan Analizi, Fırat University, Elazığ, 2016.

[41] Kömürcü, S.: Yığma Duvarların Düzlemiçi Davranışlarının Modellenmesi, İstanbul Technical University, İstanbul, 2017.

[42] Timurağaoğlu, M.Ö., Doğangün A., Livaoğlu, R.: Comparison and Assesment of Material Models for Simulation of Infilled RC Frames Under Lateral Loads, Gradevinar, 71 (2019) 1, pp. 45-56, https://doi.org/10.14256/JCE.2307.2017